Hexagonal perovskite $Sr_6(Co_{0.8}Fe_{0.2})_5O_{15}$ as an efficient electrocatalyst towards the oxygen evolution reaction
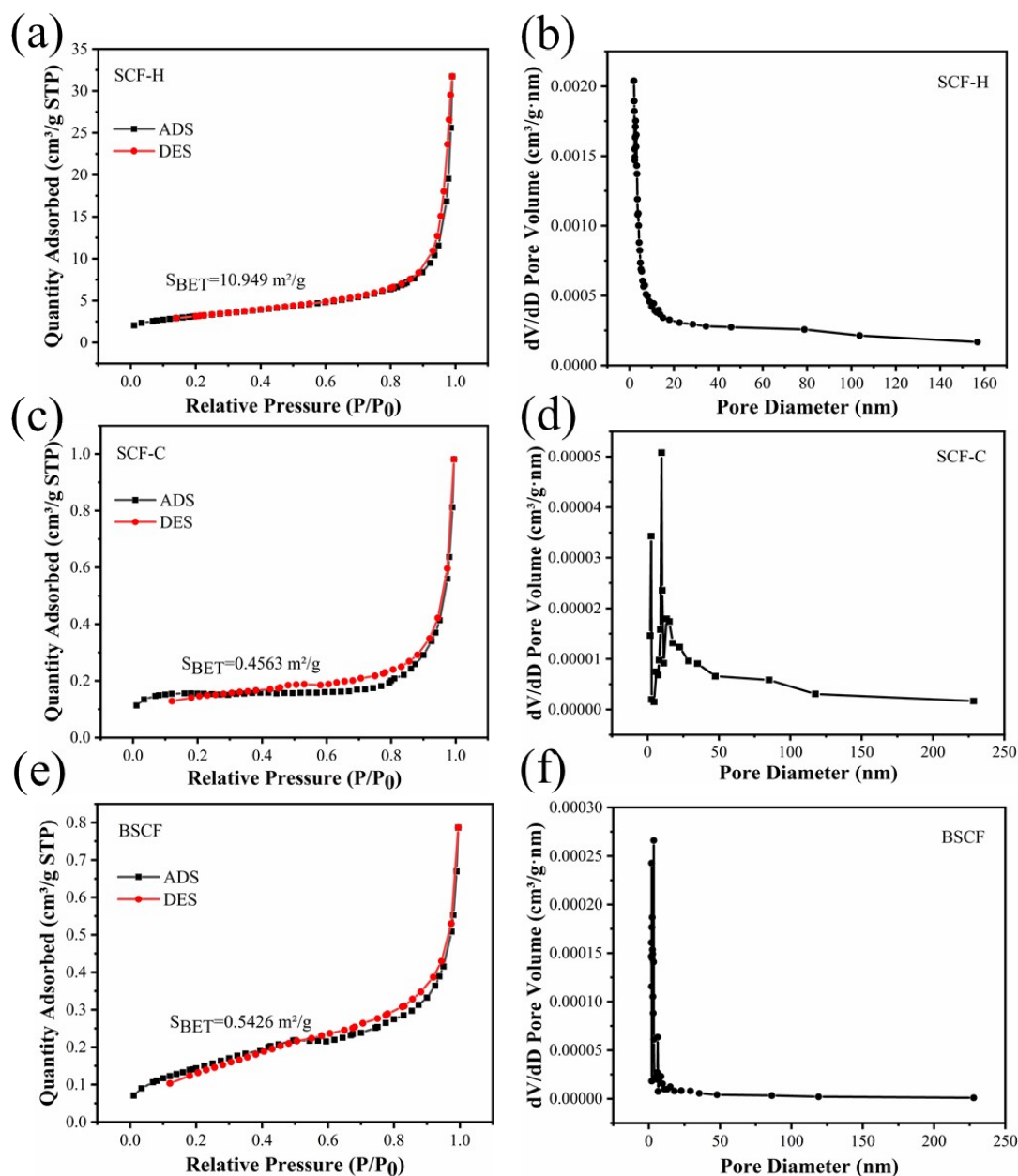

Fig. S1. The specific surface area and the pore size distribution (inside) of samples calculated based on the Brunner–Emmet–Teller (BET) method and Barrett–Joyner–Halenda (BJH) model respectively：a, b) SCF-H, c, d) SCF-C, e, f) BSCF.

Since the perovskite catalyst is usually sintered at a higher temperature, it often exhibits a low specific surface area, and the specific surface area often has a certain effect on the activity of the material. As shown in the Fig. S1, in order to obtain more microscopic information of SCF-H and SCF-C (typical BSCF added as a comparison), the specific surface area and pore structure of the catalyst are characterized by the N_2 adsorption-desorption isotherm. It can be clearly found that all samples show typical type II adsorption isotherms with hysteresis loops. The Brunner-Emmet-Teller (BET) method was used to calculate the specific surface area of the sample. The

specific surface areas of SCF-H, SCF-C and BSCF were 10.9490 m²/g, 0.4563 m²/g and 0.5426 m²/g, respectively. The BJH (Barrett-Joyner-Halenda) method was used to calculate the adsorption and desorption data to obtain the pore size distribution map. The results show that all the catalysts lacked pore structure characteristics, which is the same as the conclusion of the SEM image. Compared with SCF-C and BSCF, SCF-H exhibits a larger specific surface area, and may expose more electroactive sites, resulting in the enhancement of OER activity.
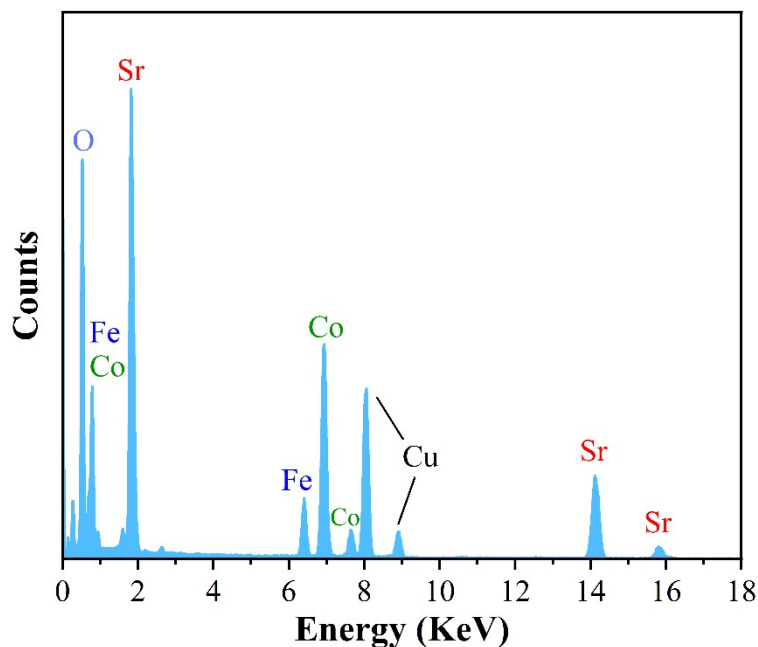

Fig. S2. EDS spectrum of SCF-H.

Table S1. Comparison of OER activity of SCF-H with reported outstanding pseudocubic perovskite-based catalysts in 1.0M KOH

| Electrocatalyst	Over-potential	Tafel	Electrode	Ref.
SCF-H	318	54	GC	This work
$PrBaCo_2O_{5.75}$	360	70	GC	[1]
$La_{0.5}Sr_{0.5}Ni_{0.4}Fe_{0.6}O_{3-\delta}$	330	76	GC	[2]
$CaLaScRuO_{6+\delta}$	478	84	GC	[3]
$CoP-PrBa_{0.5}Sr_{0.5}Co_{1.5}Fe_{0.5}O_{5+\delta}$	340	82	GC	[4]
$Sr_{0.95}Nb_{0.1}Co_{0.9-x}Ni_xO_{3-\delta}$	438	64	GC	[5]
$NdBaMn_2O_{5.5}$	430	75	GC	[6]
$La_{0.8}Sr_{0.2}CoO_{3-\delta}$-MWNT	370	-	RRDE	[7]
$La_{0.8}Sr_{0.2}Ni_{0.2}Co_{0.8}O_{3-\delta}$-MWNT	350	-	RRDE	[7]
$La_{0.9}Sr_{0.1}Fe_{0.5}Co_{0.5}O_{3-\delta}$-MWNT	330	-	RRDE	[7]
$La_{0.72}Sr_{0.28}Mn_{0.92}Co_{0.08}O_{3-\delta}$-MWNT	360	-	RRDE	[7]
$La_{0.2}Sr_{0.8}Cu_{0.4}Co_{0.6}O_{3-\delta}$-MWNT	350	-	RRDE	[7]
$La_{0.6}Sr_{0.4}Co_{0.8}Fe_{0.2}O_3$-700℃ hollow nanofibers	353	63	GC	[8]
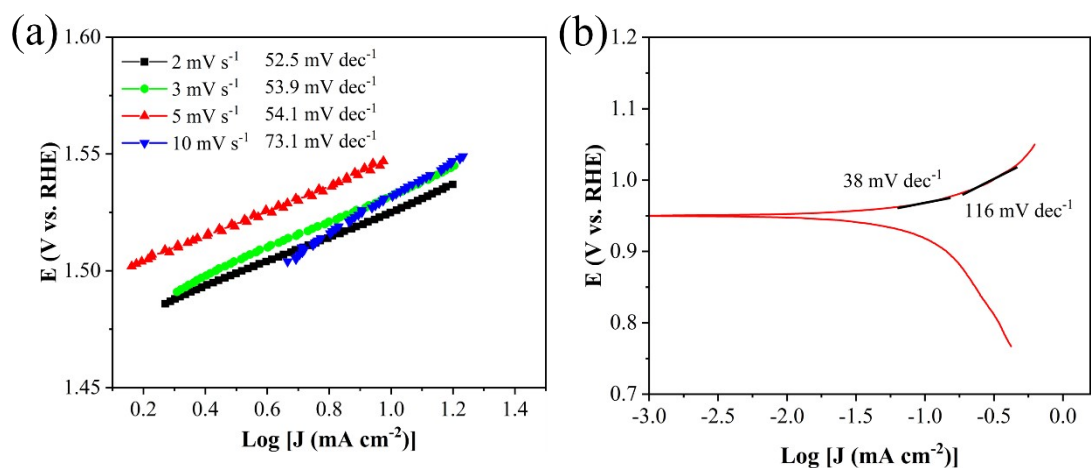
Fig. S3. a) Tafel plots and the corresponding fitted slopes for SCF-H at different scan rates. b) Tafel plot at continuous current density (from ∼0.01 to 1 mA cm^{-2}).
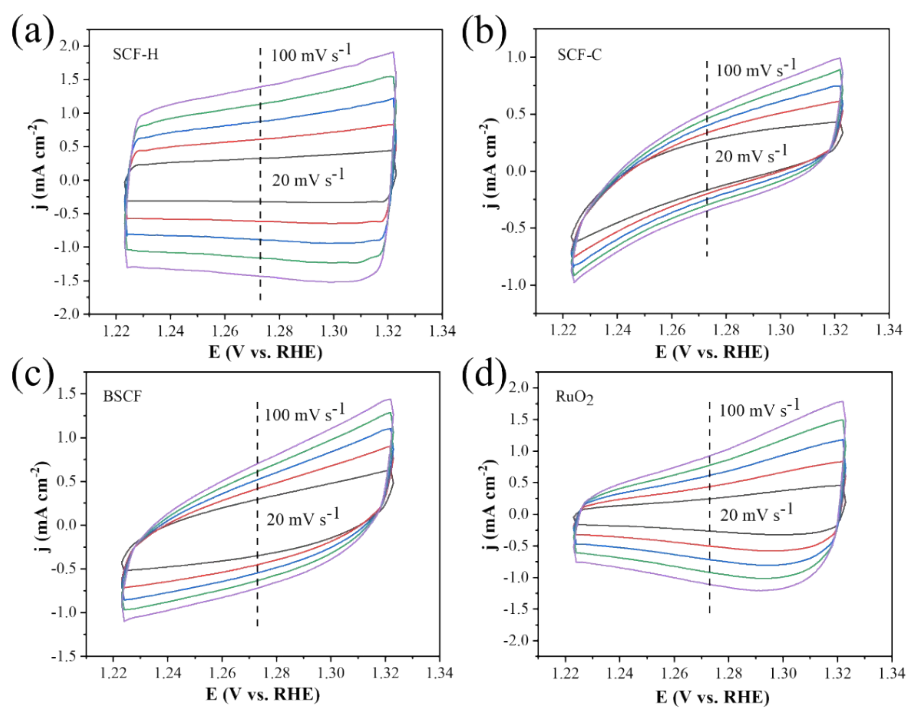

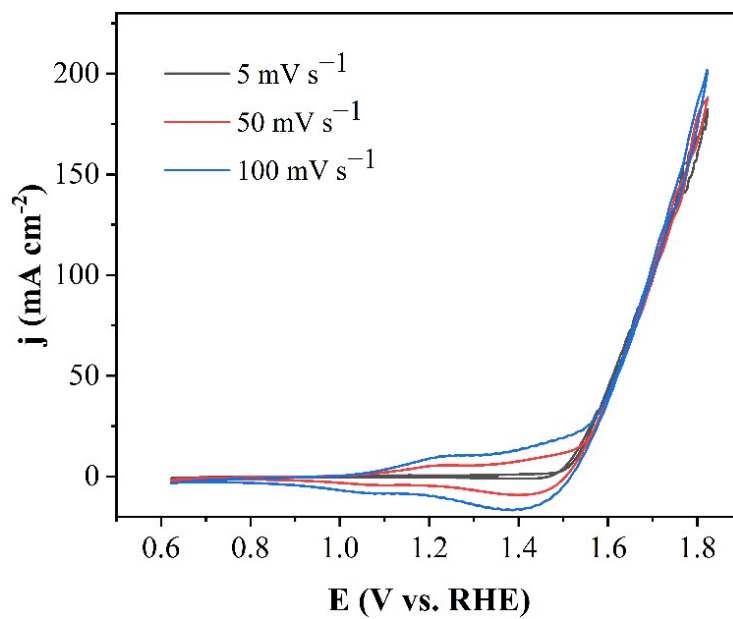**Fig. S4.** CV curves of a) SCF-H, b) SCF-C, c) BSCF, d) RuO$_2$.

Fig. S5. CV curves of SCF-H at different scan rates.
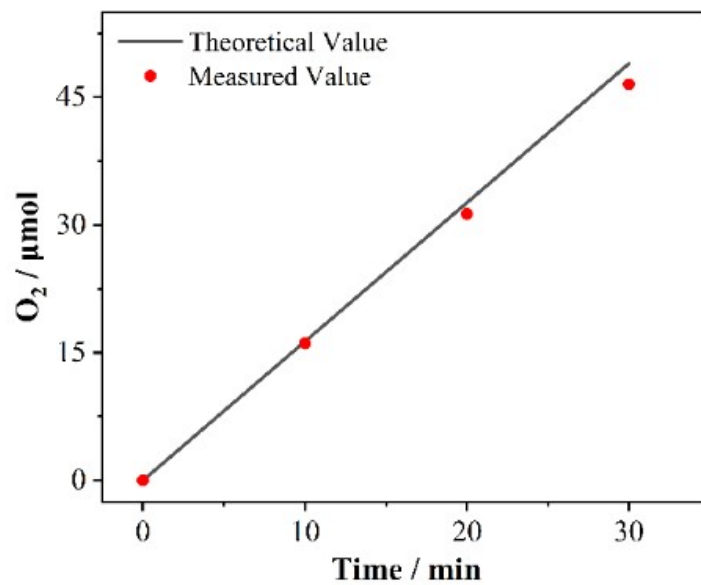

Fig. S6 Electrocatalytic efficiency of O_2 production over SCF-H.
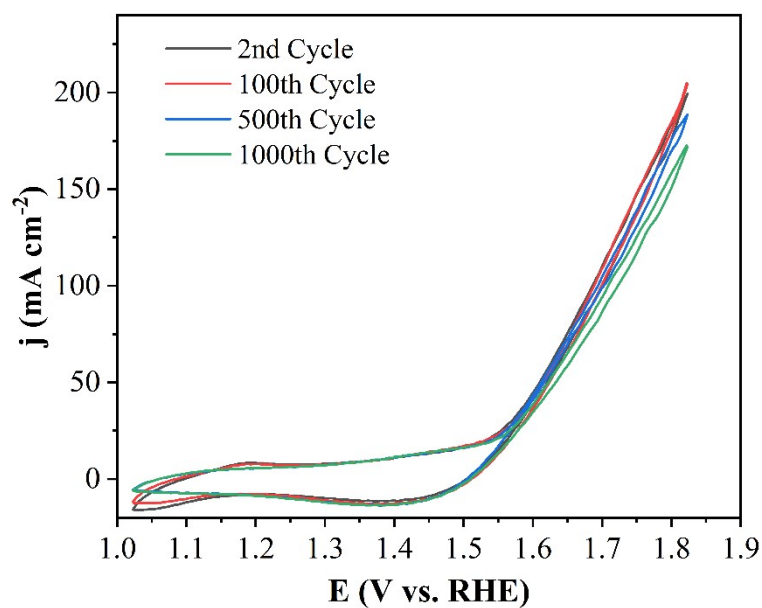
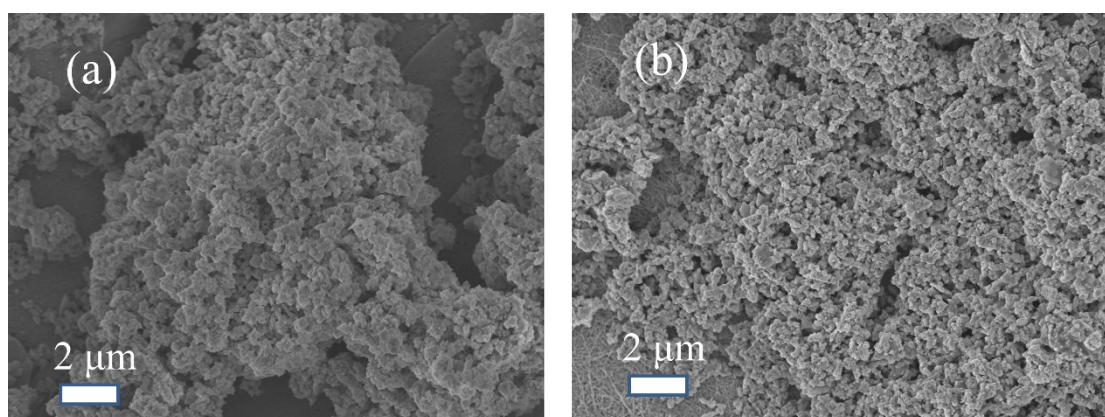**Fig. S7.** Cyclic voltammograms of SCF-H.

Fig. S8. a) SEM image of hexagonal SCF-H before OER. b) SEM image of hexagonal SCF-H after OER.
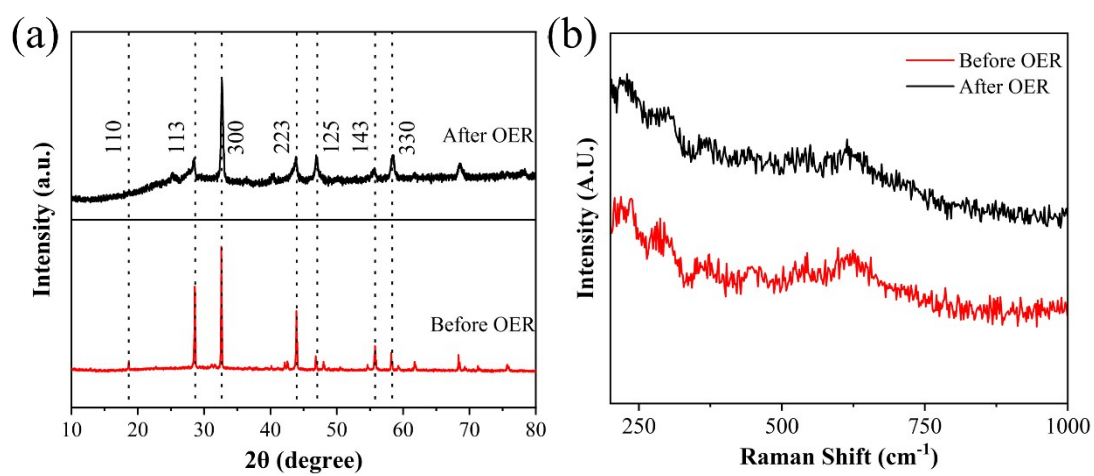

Fig. S9. a) XRD patterns of hexagonal SCF-H before and after OER. b) Raman spectra of hexagonal SCF-H before and after OER.
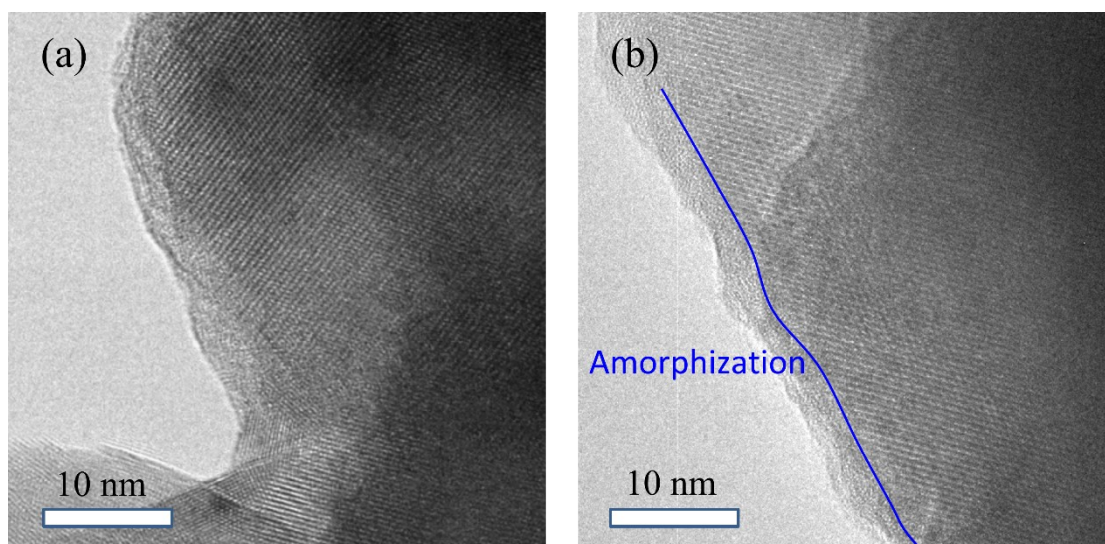
Fig. S10. a) HRTEM image of hexagonal SCF-H before OER. b) HRTEM image of hexagonal SCF-H after OER.

Table S2. The element concentration of Sr, Co and Fe in the 1 M KOH solution after cycling stability test.

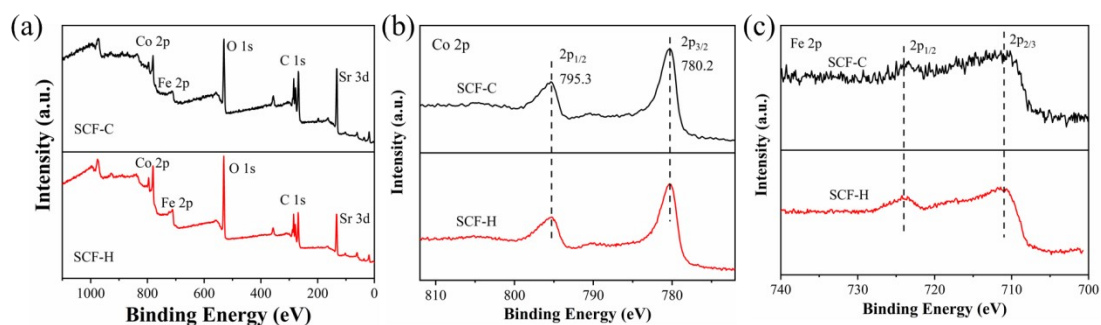| Sample	Sr element concentration(μg/L)	Co element concentration(μg/L)	Fe element concentration(μg/L)
Reference (1 M KOH)	ND	ND	ND
SCF-H (1 M KOH)	0.159	0.068	ND

ND = not detected

Fig. S11. XPS spectra of SCF-H and SCF-C: a) full spectrum, b) Co 2p, c) Fe 2p.

Computational methods:

The density functional theory (DFT) calculations were carried out using the CASTEP code of Materials Studio package of AccelrysInc[9]. The DFT exchange correlation energy was calculated using the generalized gradient approximation (GGA) method and the Perdew-Burke-Ernzerhof (PBE) functional. The ultrasoft pseudo-potentials (USP) were used for treating the core electrons. The kinetic energy cutoff was set to 400 eV for the plane-wave basis set and the self-consistent field tolerance was 1×10^{-6} eV. The Brillouin zone was sampled by 6*6*1 Monkhorst-Pack mesh k-point for surface calculation and the density of states (DOS) calculation.

REFERENCES

1. X. Miao, L. Wu, Y. Lin, X. Yuan, J. Zhao, W. Yan, S. Zhou and L. Shi, *ChemComm*, 2019, **55**, 1442-1445.

2. C. C. Wang, Y. Cheng, E. Ianni, S. P. Jiang and B. Lin, *Electrochim. Acta*, 2017, **246**, 997-1003.

3. N. Kumar, M. Kumar, T. C. Nagaiah, V. Siruguri, S. Rayaprol, A. K. Yadav, S. N. Jha, D. Bhattacharyya and A. K. Paul, *ACS Appl. Mater. Interfaces*, 2020, **12**, 9190-9200.

4. Y. Q. Zhang, H. B. Tao, Z. Chen, M. Li, Y. F. Sun, B. Hua and J. L. Luo, *J. Mater. Chem. A*, 2019, **7**, 26607-26617.

5. Q. A. Islam, R. Majee and S. Bhattacharyya, *J. Mater. Chem. A*, 2019, **7**, 19453-19464.

6. J. Wang, Y. Gao, D. J. Chen, J. P. Liu, Z. B. Zhang, Z. P. Shao and F. Ciucci, *ACS Catal.*, 2018, **8**, 364-371.

7. J. Cheng, P. Ganesan, Z. Wang, M. Zhang, G. Zhang, N. Maeda, J. Matsuda, M. Yamauchi, B. Chi and N. Nakashima, *Mater. Adv.*, 2021, **3**, 272-281.

8. L. L. Zhang, H. Zhu, J. Hao, C. Wang, Y. K. Wen, H. N. Li, S. L. Lu, F. Duan and M. L. Du, *Electrochim. Acta*, 2019, **327**, 135033.

9. S. J. Clark, M. D. Segall, C. J. Pickard, P. J. Hasnip, M. I. Probert, K. Refson and M. C. Payne, *Z Kristallogr Cryst Mater*, 2005, **220**, 567-570.